Title

Quantum chemical topology and natural bond orbital analysis of M—O covalency in M(OC 6 H 5) 4 (M = Ti, Zr, Hf, Ce, Th, Pa, U, Np)

Journal

Physical Chemistry Chemical Physics, 22(29)

ISSN

1463-9076

Authors

Berryman, Victoria EJ

Shephard, Jacob J

Ochiai, Tatsumi

et al.

Publication Date

2020-08-07

DOI

10.1039/d0cp02947e

Peer reviewed

Quantum Chemical Topology and Natural Bond Orbital Analysis of M-O Covalency in $M(OC_6H_5)_4$ (M = Ti, Zr, Hf, Ce, Th, Pa, U, Np)

Victoria E. J. Berryman,[*a] Jacob J. Shephard,[b] Tatsumi Ochiai,[c,d] Amy Price,[c] Polly L. Arnold,[c,d] Simon Parsons,[b] and Nikolas Kaltsoyannis[*a]

[a]Department of Chemistry, School of Natural Sciences, The University of Manchester, Oxford Road, Manchester, UK, M13 9PL.

[b]EaStCHEM School of Chemistry and The Centre for Science at Extreme Conditions. The University of Edinburgh, King's Buildings, West Mains Road, Edinburgh, UK, EH9 3FJ.

[c]EaStCHEM School of Chemistry, The University of Edinburgh, King's Buildings, West Mains Road, Edinburgh, UK, EH9 3FJ.

[d]Department of Chemistry, University of California, Berkeley, Berkeley CA 94720, USA. Chemical Sciences Division, Lawrence Berkeley National Laboratory, One Cyclotron Road, Berkeley 94720, USA.

Invited contribution to the **Quantum Theory: The challenge of Transition Metal Complexes** themed collection of *Physical Chemistry Chemical Physics*.

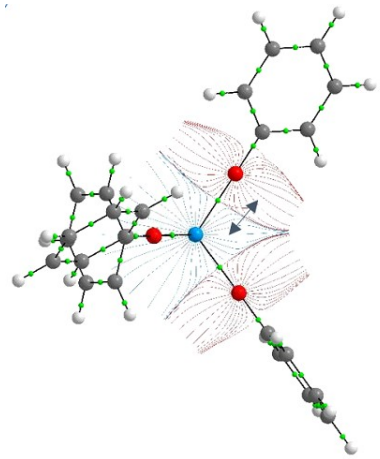

***V*$_{xc}$(M,O):** The exchange-correlation metric quantifies covalency between M and O atomic basins in $M(OC_6H_5)_4$ (M = Ti,

Abstract

Covalency is complex yet central to our understanding of chemical bonding, particularly in the actinide series. Here we assess covalency in a series of isostructural d and f transition element compounds $M(OC_6H_5)_4$ (M = Ti, Zr, Hf, Ce, Th, Pa, U, Np) using scalar relativistic hybrid density functional theory in conjunction with the Natural Bond Orbital (NBO), quantum theory of atoms in molecules (QTAIM) and interacting quantum atoms (IQA) approaches. The IQA exchange-correlation covalency metric is evaluated for the first time for actinides other than uranium, in order to assess its applicability in the 5f series. It is found to have excellent correlation with NBO and QTAIM covalency metrics, making it a promising addition to the computational toolkit for analysing metal-ligand bonding. Our range of metrics agree that the actinide-oxygen bonds are the most covalent of the elements studied, with those of the heavier group 4 elements the least. Within the early actinide series, Th stands apart from the other three elements considered, being consistently the least covalent.

Introduction

In f-element chemistry the degree of metal-ligand covalency, and in particular the role of the valence d- and f-orbitals, remains a subject of intense interest.[1–8] Although f-element bonding is predominantly ionic, understanding the covalent portion is crucial for elucidating the environmental behaviour of f-elements, advancing therapeutic applications, and for the design and optimization of ligands for effective separation processes in the nuclear fuel cycle.

Quantum chemical topology (QCT) is a field within theoretical chemistry that partitions chemical systems from quantitative evaluation of quantum mechanical functions. For a comprehensive review of QCT see reference 9. An important feature of QCT methods is the parameter-free nature of the partitioning. Many bonding descriptions suffer from dependence on orbital-based definitions which vary with methodology, and relating these bond descriptions to bond energy is sometimes difficult and not rigorous. Herein we employ perhaps the most well-known part of QCT, Bader's quantum theory of atoms in molecules (QTAIM) methodology, and the less well-known Interacting Quantum Atoms (IQA) approach, an energy decomposition scheme for energy and charge partitioning of molecular systems. IQA partitions the molecule using the same formalism as QTAIM, calculating the energy from the first- and second-order density matrices. It is independent of the atomic virial theorem and is thus particularly useful in non-equilibrium systems. A formal equivalent of Bader's QTAIM methodology, IQA allows for the decomposition of the bond energy into atomic self-energies and interaction energy terms.[10–13] It provides a method to unite bond metrics and the energetics of a bonding interaction via the real-space approach, and the atomic self-energies and interaction energy terms can in principle be measured experimentally.[14]

Techniques based on real-space analysis provide metrics for any pair of atoms in a system. In this way interactions between atoms do not depend on the debated concept of where a chemical bond exists. Within the IQA framework, the interatomic interaction energy between two atoms, A and B, is denoted $V_{\mathrm{Inter}}(\mathrm{A,B})$ and can be partitioned into its electrostatic and exchange-correlation contributions such that

$$\mathrm{V_{Inter}(A,B)} = \mathrm{V_{Elec}(A,B)} + \mathrm{V_{XC}(A,B)} \quad (1)$$

where $V_{\mathrm{Elec}}(\mathrm{A,B})$ is the electrostatic or ionic contribution and $V_{\mathrm{XC}}(\mathrm{A,B})$ is the exchange-correlation or covalent contribution to the interaction. The former includes the nuclear-nuclear repulsive energy, electron-nuclear attraction energies and the Coulombic portion of the electron-electron repulsion energy. It has been demonstrated that the

exchange-correlation components, as opposed to the electrostatic contributions, best describe chemical bonds.[15] Thus, herein we assess this component of the interatomic interaction energies.

We previously reported a computational assessment of the covalency in the metal-oxygen bond of the d and f transition element complexes $M(OC_6H_5)_4$ (M = Ti, Zr, Hf, Ce, Th and U).[16] This contribution extends that work to include the additional actinides Pa and Np, thereby allowing us to survey all four early actinides from Th to Np. We explore covalency using both natural localised molecular orbital- and QCT-based analysis tools, including V_{XC}, which we have not previously employed. Our aim is to establish the best metrics for quantifying metal-ligand covalency, especially in the 5f series.

Methods

The Gaussian 16 software package, revision A.03, was used for all density functional theory (DFT) calculations.[17] Consistent with our previous study[16], the hybrid density functional approximation, PBE0,[18,19] was used with Grimme's D3[20] and the Becke-Johnson damping parameters for dispersion corrections.[21–23] Dunning's correlation consistent basis sets of polarized triple-ζ quality were employed for non-metal atoms (H, C and O).[24–27] Small-core Stuttgart-Bonn relativistic effective core potentials (ECP) replace the 60 core electrons of Pa and Np, and the associated segmented valence basis sets are used.[28–30] This is consistent with the approach used for the actinide atoms in our previous work. Geometry optimizations of the systems were performed in C_2 symmetry. Subsequent calculations which explore the effect of shortening *r*(M-O) employed opt=modredundant to constrain only the *r*(M-O) parameter and allow all other atom parameters to be optimized. Default settings were used for the optimizations. Analysis of the harmonic vibrational frequencies confirmed the optimized geometries as energetic minima.

Natural Localized Molecular Orbitals (NLMOs) were computed with the NBO 7.0 software package.[31] The CHOOSE option was employed to impart a consistent bonding scheme in all systems, which allowed for comparison of analogous overlap integrals in M–O bonding. Electron density-based analysis of metal–ligand bonding utilized the AIMAll software package,[32] using the WFX files generated from the DFT calculations (in Gaussian 16). For the Ti, Zr, Hf, Ce, Th, and U systems, the WFX files were generated in

our previous study.[16] The WFX files were edited to include the <Model> tag to designate 'Unrestricted PBE0' and IQA analysis was invoked in AIMAll using encomp=4.[¶]

[¶¶] Currently, IQA does not include relativistic effects in the atomic energies, irrespective of whether a relativistic Hamiltonian or a pseudopotential is employed. This results in discrepancies in the total molecular energy computed with IQA. However, the accuracy of one-electron and two-electron properties, such as V_{XC}, are not dependent on the reproduction of the total energy via IQA,[42] and these metrics have been previously applied to actinide systems.[35]

Results and Discussion

Our previous study probed the bonding in a series of $M(OC_6H_5)_4$ systems, where M = Ti, Zr, Hf, Ze, Th, U, and how it changes as the M-O bond distance is shortened in 0.02 Å increments to a maximum of -0.12 Å from the optimized *r*(M-O). These structural distortions were studied as we have an ongoing experimental programme to probe the effects of pressure on metal-ligand bonding,[33] and the shortening of bonds is one possible consequence of the application of pressure to molecular crystals. Here we expand the systems studied to include Pa and Np. This completes the early actinides from Th to Np, allowing us to quantify systematically the effects of the changing metal valence atomic orbital energies and radial distributions on the covalency metrics.

The structural parameters of the optimized $Pa(OC_6H_5)_4$ and $Np(OC_6H_5)_4$ systems, together with those previously studied, are shown in Table 1. Shortening of *r*(M-O) by -0.12 Å results in minimal structural changes, e.g. modest increases to M-O-C angles of 1.3° for $Pa(OC_6H_5)_4$ and 3.6° for $Np(OC_6H_5)_4$, and increase to the O-M-O angles of 0.5° for $Pa(OC_6H_5)_4$ and 2.0° for $Np(OC_6H_5)_4$.

The deformation energies of $M(OC_6H_5)_4$ with changes in *r*(M-O) are shown in Figure 1. The d-element systems show the largest changes in energy upon shortening of *r*(M-O), with Ti > Hf > Zr. This is followed by the actinides, which lie within 1 $kJ{\cdot}mol^{-1}$ of one another, and finally the lanthanide system, $Ce(OC_6H_5)_4$. Overall, the trend is Ti > Hf > Zr > Th ≈ Pa ≈ U ≈ Np > Ce.

Table 1. Optimized structural parameters for $M(OC_6H_5)_4$. All structures have C_2 symmetry and values are reported as averages (the maximum difference in the lengths of the two pairs of symmetry-related M-O bonds is 0.001 Å). ∠(O-M-O) is reported as the angle between closest ligand pairs, *i.e.* the narrowest of the ∠(O-M-O). Data for $M(OC_6H_5)_4$ (M = Ti, Zr, Hf, Ce, Th and U) from reference 16.

Compound	***r*(M-O), Å**	**∠(M-O-C), °**	**∠(O-M-O), °**
$Ti(OC_6H_5)_4$	1.785	171.0[†]	108.8
$Zr(OC_6H_5)_4$	1.937	172.0	109.7
$Hf(OC_6H_5)_4$	1.919	170.1	109.5
$Ce(OC_6H_5)_4$	2.086	172.4	105.2
$Th(OC_6H_5)_4$	2.147	177.4	107.9
$Pa(OC_6H_5)_4$	2.101	177.4	107.7
$U(OC_6H_5)_4$	2.088	172.5	102.4
$Np(OC_6H_5)_4$	2.080	170.2	105.1

[†]Ti-O-C angle fixed to the average of the Zr-O-C and Hf-O-C angles, as discussed in reference 16.

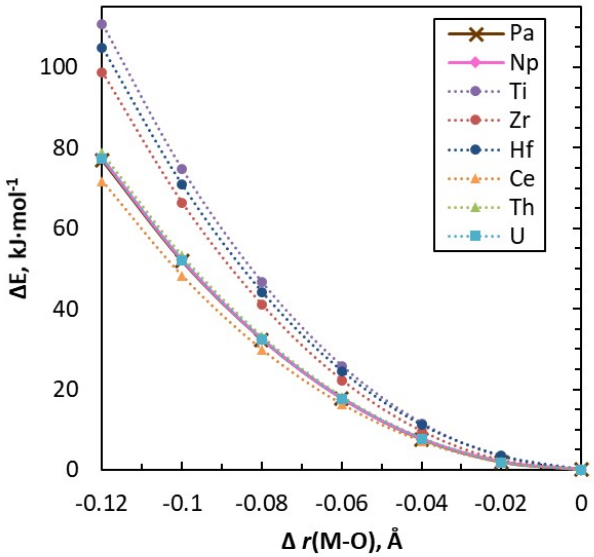

Figure 1. Relative energy changes for $M(OC_6H_5)$ as a function of *r*(M-O). Data for $M(OC_6H_5)_4$ (M = Ti, Zr, Hf, Ce, Th and U) from reference 16. The previously reported systems are shown as dotted lines. $Pa(OC_6H_5)_4$ and $Np(OC_6H_5)_4$ are shown as solid brown and pink lines, respectively.

Natural localized molecular orbital analysis

The natural localized molecular orbitals (NLMOs) are defined within the NBO framework, and enforce integer occupancy. They have the advantage of being more localized than typical canonical orbitals, representing a more 'Lewis-like' structure and a conceptually intuitive picture of chemical bonding. The NLMOs are a complete and orthonormal set, each associated with a corresponding pre-orthogonal set of hybrid orbitals (PNHO), the overlap of which can also be assessed within the NBO program.

The M-O bond in the $M(OC_6H_5)_4$ complexes is described by three NLMOs: one σ-type and two π-type, which are shown in Figure 2 for $Pa(OC_6H_5)_4$ and $Np(OC_6H_5)_4$. The orbitals are similar to those of the other systems studied previously, and allow for a meaningful comparison of the effects of the central metal atom on bonding.

We have decomposed the NLMOs to obtain the contribution from the metal atom (%M) to M-O bonding. The results are shown as the sum of the 3 bonding orbitals (σ + 2π) as a function of *r*(M-O) in Figure 3. The σ and π contributions are shown separately in Figure S1. All NLMOs individually have less than 15% metal character and thus are highly polarized. For the actinides, the %M contribution increases periodically (*i.e.* monotonically across the 5f period) such that Th < Pa < U < Np. The overall trend for the systems considered herein is Th < Zr < Hf < Ce ≈ Pa < U < Np < Ti. The %M contribution from $Pa(OC_6H_5)_4$ is approximately equal to that of Ce, yet increases to a

greater extent with the shortening of *r*(M-O). The Pa, U and Np systems exhibit the greatest changes in %M over the range of *r*(M-O) distances studied, increasing 20 – 90 % more steeply than the other systems. The %M increase for Pa, U and Np is greatest for both σ and π bonding, however the effect is more dramatic in the case of π bonding where the %M contributions increase by *ca.* 2 to 4 times that of the other systems.

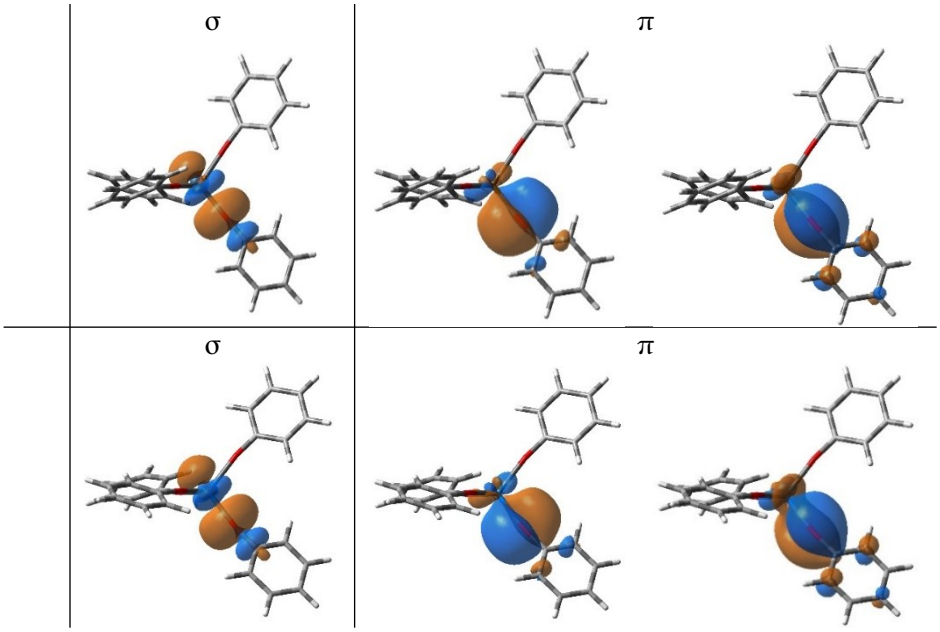

Figure 2. The M-O bonding NLMOs in $Pa(OC_6H_5)_4$ (top), and $Np(OC_6H_5)_4$ (bottom). The σ-type and two π-type orbitals are shown, from left to right, for one M-O interaction. Isosurface value of 0.02 au. All four M-O interactions have one σ and two π NLMOs.

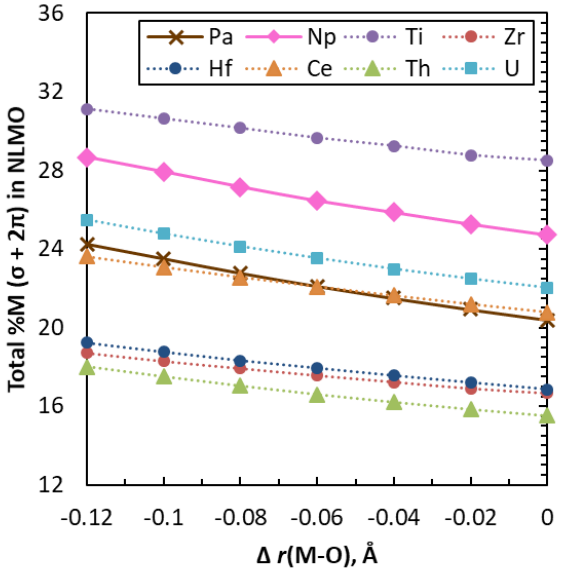

Figure 3. Sum (σ + 2π) of metal contribution (%M) to the M-O bonding NLMOs as a function of *r*(M-O) in $M(OC_6H_5)_4$. Individual σ and π contribution are provided in Figure S1. Data for $M(OC_6H_5)_4$ (M = Ti, Zr, Hf, Ce, Th and U) from reference 16.

The NLMOs can be further decomposed into the metals' atomic orbital character, shown in Figure 4. In each case, the σ and average π orbital composition is shown as a function of orbital character and as a percentage of the total contribution to the NLMO. The results are shown for the optimized system and where *r*(M–O) is shortened by −0.12 Å. In the σ-type bonding orbitals, all systems exhibit predominantly d character, with minor contributions from s and f orbitals. Interestingly, there is a consistent decrease in f character across the actinides from Th to Np. Conversely, the π-type bonding orbitals show a consistent increase in f character as the actinide series is traversed. This trend is also present in d character, but to a lesser extent. Our data are consistent with those of Vallet *et al.* for Pa peroxo-clusters $[Pa_4O(O_2)_6F_{12}]^{6-}$, and hexametalates $Pa_6O_{19}^{8-}$, which feature equal 5f and 6d orbital participation in the π-type orbitals, and increased 5f orbital character in the U analogues.[34]

In our previous study, we found a correlation between the d character of the M-O bonds with the deformation energy of the system (R^2 = 0.72). With the addition of the Pa and Np systems, a similar correlation is found (R^2 = 0.71), which is stronger for the π-type NLMOs (R^2 = 0.75) than the σ-type (R^2 = 0.60) and is shown in Figure S2. In the actinides, there is poor correlation between the f character in the NLMOs and deformation energy (R^2 = 0.42), shown in Figure S3, indicating that f character does not significantly affect the deformation energy of the M-O bond.

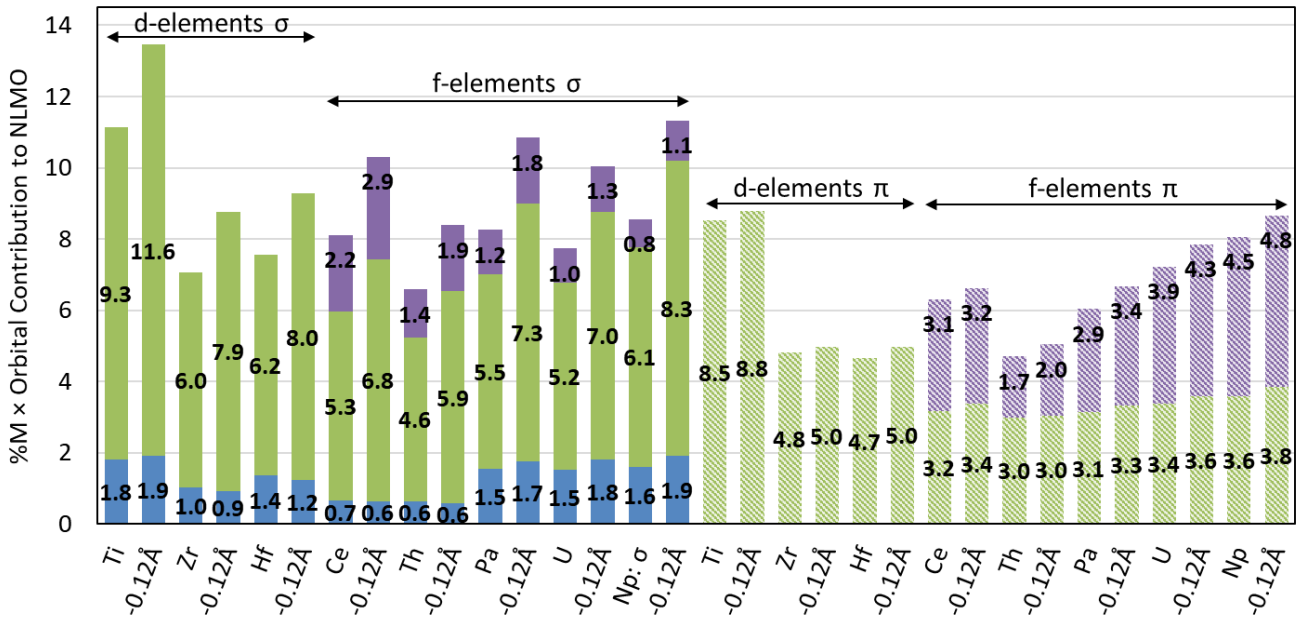

Figure 4. The %M contribution to M-O bonding NLMOs in optimized $M(OC_6H_5)_4$ and at [r(M-O) – 0.12 Å]. s, d, and f character is represented by blue, green, and purple colours, respectively. The σ- and π-type NLMOs are shown as solid and striped bars, respectively. The π-type NLMO data are averages of the two π-type NLMOs. Values

≤0.01% are not shown. Data for $M(OC_6H_5)_4$ (M = Ti, Zr, Hf, Ce, Th and U) from reference 16.

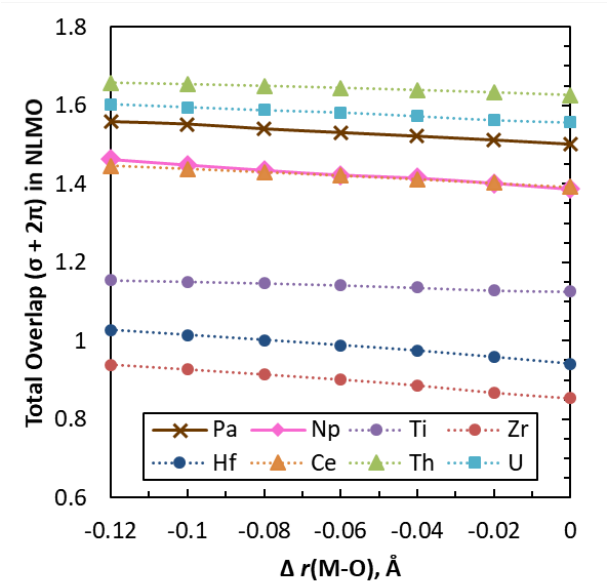

Figure 5. Sum (σ + 2π) of overlap in the M-O bonding NLMOs as a function of *r*(M-O) in $M(OC_6H_5)_4$. Data for $M(OC_6H_5)_4$ (M = Ti, Zr, Hf, Ce, Th and U) from reference 16.

To further assess the nature of the M-O bonds, the overlap of the precursor PNHOs that form the NLMOs were analysed and the results are shown in Figure 5. By contrast to the increase in %M across the actinide series, the overlap tends to decrease, though this is not periodic for the actinides, with an overlap trend for the actinides of Th > U > Pa > Np. Mindful of the possible effect on overlap of M-O-C angle (Table 1), the U and Np systems were re-evaluated at the near-linear M-O-C angle of the Th and Pa systems (177.4°). This led to modest decreases in M-O overlap but the overall trend remained the same, *i.e.* Th > U > Pa > Np ≈ Ce > Ti > Hf > Zr.

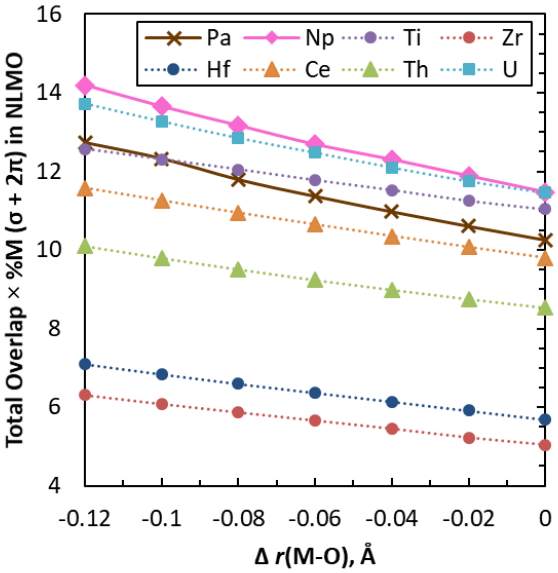

Figure 6. Product of the overlap integrals and %M contributions to the three M-O bonding NLMOs ($\sigma + 2\pi$) as a function of r(M-O) in $M(OC_6H_5)_4$. Data for $M(OC_6H_5)_4$ (M = Ti, Zr, Hf, Ce, Th and U) from reference 16.

We have shown that it is useful to incorporate both the %M contribution and the overlap of the precursor PNHOs that form the NLMOs to describe M-O bonding.[16] This previously-introduced covalency metric is the product of %M and the overlap, and is shown in Figure 6 as a total of the σ- and 2 π-type NLMOs. The overall trend is Np > U > Ti > Pa > Ce > Th > Hf > Zr. For the actinides, the trend is now periodic, and it is noteworthy that the f elements exhibit the greatest change in the covalency metric over the range of r(M-O) distances.

Atomic charges

The partial atomic charges from QTAIM and from natural population analysis (NPA) within the NBO framework are shown in Table 2 for the metal and oxygen atoms. Both sets of atomic charges show deviation in the charge on the metal from the formal 4+ oxidation state, suggesting ligand-to-metal charge transfer in all complexes. Decreased charge, and charge separation, is associated with covalency, and for the actinides, q(M) suggests an increase in covalency as the group is traversed. In our previous study, we showed consistency between the QTAIM and NPA charge trends, and this still holds when our additional actinide data are included. For the actinide systems, there are correlations between the QTAIM and NPA trends for q(M), q(O) and [q(M) – q(O)], of $R^2 = 0.95$, $R^2 = 0.94$, and $R^2 = 0.95$, respectively.

Table 2. QTAIM and NPA atomic charges q for the optimized $M(OC_6H_5)_4$ systems. Data throughout shortening of r(M-O) are shown in Table S1. Data for $M(OC_6H_5)_4$ (M = Ti, Zr, Hf, Ce, Th and U) from reference 16.

	QTAIM		NPA	
Compound	***q*(M)**	***q*(O)**	***q*(M)**	***q*(O)**
$Ti(OC_6H_5)_4$	2.33	-1.23	1.70	-0.68
$Zr(OC_6H_5)_4$	2.68	-1.29	2.66	-0.89
$Hf(OC_6H_5)_4$	2.74	-1.31	2.65	-0.89
$Ce(OC_6H_5)_4$	2.49	-1.24	2.07	-0.75
$Th(OC_6H_5)_4$	2.84	-1.30	2.69	-0.90
$Pa(OC_6H_5)_4$	2.72	-1.29	2.31	-0.82
$U(OC_6H_5)_4$	2.63	-1.27	2.25	-0.80
$Np(OC_6H_5)_4$	2.56	-1.25	2.05	-0.76

Quantum chemical topology analysis

QTAIM and IQA data are summarized in Table 3. QTAIM metrics have been used extensively in the literature to quantify chemical bonding and have been shown to be particularly useful in f-element chemistry. IQA extends the QTAIM framework and has only very recently been applied to the actinides, specifically to quantify covalency in $[E{=}U{=}E]^{2+}$ (E = O, S, Se, Te) and $[UE_2(H_2O)_5]^{2+}$ via the V_{XC}(U,E) metric.[35] Here we extend the application of this metric to further explore covalency in the 5f elements.

Table 3. QTAIM and IQA metrics (in au) for the optimized $M(OC_6H_5)_4$ systems. Metrics for *r*(M-O) shortened to -0.12 Å are shown in Table S2. Data for $M(OC_6H_5)_4$ (M = Ti, Zr, Hf, Ce, Th and U) from reference 16.

Compound	***r*(M-O), Å**	ρ_{BCP}	$\nabla^2\rho_{BCP}$	$-(G_{BCP}/V_{BCP})$	H_{BCP}	**δ(M, O)**	**V_{XC}(M, O)**
$Ti(OC_6H_5)_4$	1.785	0.146	0.762	0.836	-0.047	0.766	-0.176
$Zr(OC_6H_5)_4$	1.937	0.119	0.644	0.863	-0.030	0.687	-0.150
$Hf(OC_6H_5)_4$	1.919	0.130	0.757	0.856	-0.033	0.666	-0.149
$Ce(OC_6H_5)_4$	2.086	0.112	0.426	0.796	-0.037	0.822	-0.173
$Th(OC_6H$	2.147	0.10	0.39	0.795	-	0.744	-0.160

$_5)_4$		7	2		0.034		
$Pa(OC_6H_5)_4$	2.101	0.124	0.448	0.773	-0.046	0.856	-0.183
$U(OC_6H_5)_4$	2.088	0.125	0.482	0.786	-0.045	0.856	-0.184
$Np(OC_6H_5)_4$	2.080	0.124	0.503	0.791	-0.045	0.858	-0.184

The QTAIM metrics ρ_{BCP}, $\nabla^2\rho_{BCP}$, $-(G_{BCP}/V_{BCP})$, and H_{BCP} characterise the bond critical point along the M-O bond path, and can be used to quantify M-O covalency. ρ_{BCP} and H_{BCP} are, respectively, the electron and energy densities at the BCP; a general rule is that interactions with $\rho_{BCP} > 0.2$ au and $H_{BCP} < 0$ are the result of significant electron sharing and are thus considered covalent in nature,[36,37] while $\rho_{BCP} < 0.1$ au is typical of ionic interactions. Very few BCPs involving actinide atoms exceed a ρ of 0.2 au, and are frequently less than 0.1 au, so the ρ_{BCP} and H_{BCP} values for our target systems do suggest some degree of covalency. The values of ρ_{BCP} for all systems are shown in Figure 7, as a function of the shortening of r(M-O). For the actinides, there is the least electron density in the internuclear region for Th, followed by U, Pa, and Np, which have strikingly similar ρ_{BCP}. The H_{BCP} data also differentiate Th from Pa-Np. Although the NLMO data show significant increases in the 5f contribution to the π orbitals across the early actinides, ρ_{BCP} is affected much more strongly by σ bonding; Fig. 4 shows that the metal contribution to the Th-O σ bond at r_{eqm} is less than for the other three An-O, which are about the same as one another.

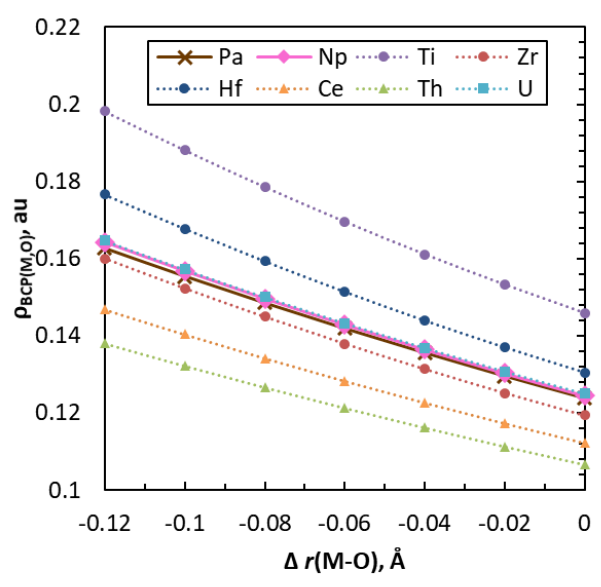

Figure 7. The electron density at the M-O BCP, ρ_{BCP}, for the $M(OC_6H_5)_4$ systems with changes in r(M-O). Data for $M(OC_6H_5)_4$ (M = Ti, Zr, Hf, Ce, Th and U) from reference 16.

The Laplacian of ρ_{BCP}, $\nabla^2\rho_{BCP}$, describes the degree of electron density concentration ($\nabla^2\rho_{BCP} < 0$) or depletion ($\nabla^2\rho_{BCP} > 0$) at the BCP. Although, in general, covalent interactions have negative $\nabla^2\rho_{BCP}$, highly polarized bonding also yields positive values of $\nabla^2\rho_{BCP}$.[37] The NLMO analysis confirms the highly polarized nature of the M-O bonds, and all our systems have a positive $\nabla^2\rho_{BCP}$. The magnitude of $\nabla^2\rho_{BCP}$ is less for the actinides than for the d elements, and the trend is periodic, increasing across the series from Th to Np.

Electron delocalization leads to attenuation of kinetic energy density, and it has been previously shown that the ratio $-(G_{BCP}/V_{BCP})$ can provide a measure of covalency.[16,38] Since our systems have positive $\nabla^2\rho_{BCP}$, the $-(G_{BCP}/V_{BCP})$ ratio must be $\geq$ 0.5. Interactions where $-(G_{BCP}/V_{BCP})$ is between 0.5 and 1 have covalent character, while above 1 are considered to be non-covalent. As with $\nabla^2\rho_{BCP}$, the magnitude of $-(G_{BCP}/V_{BCP})$ is smaller for the f elements than the transition metals (Figure S4), which is consistent with the greater overlap metrics for the f elements in the NLMO analysis, as greater orbital overlap brings about a decrease in the kinetic energy density of the interaction. Overall, the $-(G_{BCP}/V_{BCP})$ metric suggests a covalency trend of Pa > U > Np > Th ≈ Ce > Ti > Hf > Zr, with Th-O again being the least covalent actinide bond.

The final QTAIM metric we consider is the delocalization index, δ(M,O). This is a so-called integrated property as it is evaluated not at a single point in space, but between atomic basins. It provides a measure of the number of electron pairs shared between atoms and is directly related to the bond order, irrespective of the nature of the interaction. The changes in the delocalization indices for the shortening of r(M-O) are presented in Figure 8. As with ρ_{BCP} and H_{BCP}, the Pa, U, and Np systems have similar δ(M,O), with an overall trend of Np ≈ U ≈ Pa > Ce > Ti > Th > Zr > Hf. Th is once again the least covalent 5f element.

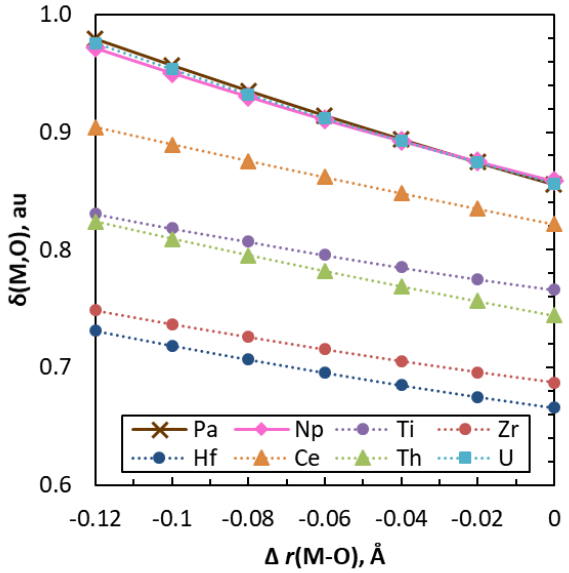

Figure 8. The delocalization index, δ(M,O), for the $M(OC_6H_5)_4$ systems with changes in r(M-O). Data for $M(OC_6H_5)_4$ (M = Ti, Zr, Hf, Ce, Th and U) from reference 16.

As discussed in the Introduction, the IQA definition of the interaction energy includes an exchange correlation interaction term, denoted V_{XC}, that describes the degree of covalency for the interaction between any pair of atoms. The results for the M-O bond in the $M(OC_6H_5)_4$ system are shown in Table 3 at r_{eqm}, and Figure 9 over the shortening of r(M-O). A more negative value of V_{XC}(M,O) indicates a greater degree of covalency, and so the transthorium actinides are found to be the most covalent of all the target systems. Previous studies show tetravalent cerium systems have greater covalency than thorium, and less than their uranium analogues. The IQA metric supports this U > Ce > Th covalency trend.[39,40] The IQA data are similar to ρ_{BCP}, H_{BCP} and δ(M,O), in that the Pa, U and Np systems exhibit very similar covalency, differentiating them from Th. Overall, V_{XC}(M,O) gives a covalency trend of Pa ≈ U ≈ Np > Ti > Ce > Th > Zr > Hf.

The slope of V_{XC}(M,O) as a function of r(M-O) varies with M, the rate of change being 15-40 % greater for Pa, U, and Np compared to the other systems, reminiscent of the behaviour of %M in the NLMO analysis. In other words, V_{XC}(M,O)-defined covalency increases more rapidly for the Pa, U, and Np systems as r(M,O) is shortened. These systems have significant f character in the bonding and the additional angular node, relative to the d elements, may facilitate greater increases in V_{XC} with decreased r(M,O), as may their accessing the maximum in the 5f radial distribution as r(M,O) is shortened.

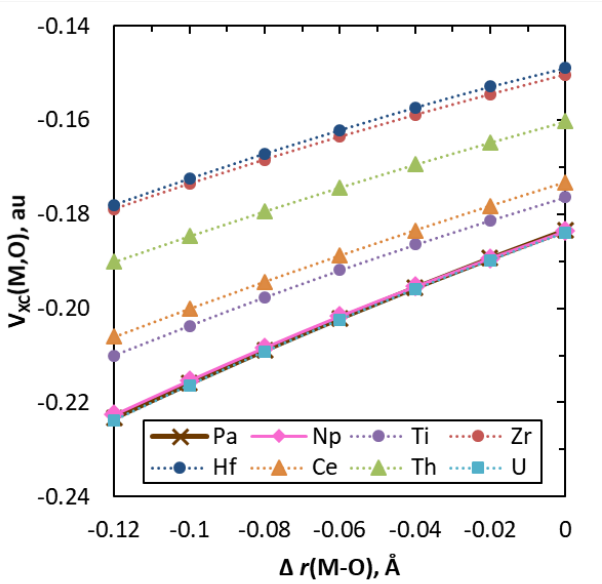

Figure 9. The IQA covalency metric, V_{XC}(M,O), for the M-O bond in the M(OC$_6$H$_5$)$_4$ systems with changes in r(M-O).

Consistency between the covalency metrics

While it is probably unrealistic to expect all the covalency metrics to provide a unified description of metal-ligand bonding, correlations between them give confidence in the methods and reported trends. In our previous work we identified the %M × overlap, –(G_{BCP}/V_{BCP}), and δ(M,O) metrics as key for predicting covalency. We now extend these to include the V_{XC}(M,O) metric, Table 4. Correlations between all metrics in Table 4 were considered and R^2 values between 0.44 and 0.92 were obtained, and are shown in Figure S5. Our previous study reported the best correlation between the NLMO metric, %M × overlap, and the QTAIM delocalization index, δ(M,O). When Pa and Np are included there is again a good correlation (R^2 = 0.80) between these metrics. –(G_{BCP}/V_{BCP}) exhibits the weakest correlation with the other metrics. As our previous study mentioned, this metric focuses on a single point in the internuclear region and is most significantly impacted by σ-type interactions. Since many of the systems differ most substantially in π-type bonding interactions (Figure S1), this may account for the greater deviation in the –(G_{BCP}/V_{BCP}) metric from the others. The best correlations (R^2 = 0.92) are found between the V_{XC}(M,O) metric and both the NLMO metric %M × overlap and the delocalization index δ(M,O). These correlations are shown in Figure 10. It is noticeable that Ti has the largest variation in position in the covalency trends, although always emerges as the most covalent of the group 4 elements. This is also supported by the partial charge data in Table 2. We discussed the position of Ti in these trends at some length in our previous study[16] and we direct the interested reader to that.

Table 4. Covalency trends for selected covalency metrics for the M-O bond in the $M(OC_6H_5)_4$ systems.

Metric	Covalency trend
NLMO: %M × overlap	Np > U > Ti > Pa > Ce > Th > Hf > Zr
QTAIM: $-(G_{BCP}/V_{BCP})$	Pa > U > Np ≥ Ce ≈ Th > Ti > Hf > Zr
QTAIM: δ(M,O)	Pa ≈ U ≈ Np > Ce > Ti > Th > Zr > Hf
IQA: V_{XC}(M,O)	Pa ≈ U ≈ Np > Ti > Ce > Th > Zr > Hf

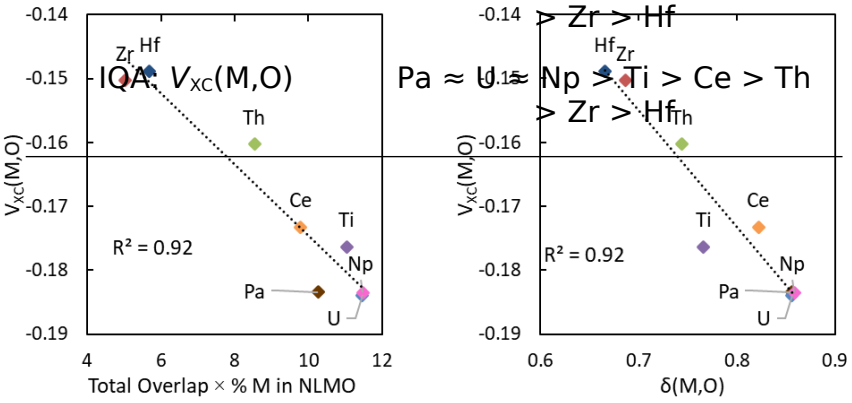

(a) (b)

Figure 10. The covalency metrics (from Table 4) which display the best correlations with one another. Data for $M(OC_6H_5)_4$ (M = Ti, Zr, Hf, Ce, Th and U) from reference 16.

None of the covalency metrics correlates well with the deformation energy of the complexes (the energy difference between the systems at r_{eqm} and when shortened by 0.12 Å, see Figure S6), with the possible exception of $-(G_{BCP}/V_{BCP})$, for which R^2 = 0.76. This may well reflect the rather modest levels of covalency in all these target systems, and hence that the bonding energy is determined more by ionic factors which are not well captured by the metrics given in Table 4.

Finally, we note that a reviewer asked us about the relationship between the methods used in this work to the Ziegler-Rauk energy decomposition scheme implemented in the Amsterdam Density Functional code, noting the scheme's extensive use in transition metal and actinide chemistry. In the present work we have not employed the Ziegler-Rauk scheme so clearly cannot comment directly on its performance for the title complexes, but are very happy to direct the reviewer, and the interested reader, to our 2013 comparison of QTAIM and energy decomposition data on other transition metal and actinide molecules.[41]

Conclusions

In this study, we introduce V_{XC} as a measure of M-O covalency in $M(OC_6H_5)_4$ (M = Ti, Zr, Hf, Ce, Th, Pa, U, Np) and compare it with a range of other established electron density topology and molecular orbital-based covalency metrics, finding it to show excellent correlation ($R^2 > 0.9$) with both M-O delocalisation indices and NLMO character. Application of V_{XC}, and other metrics, leads to the conclusion that within our target systems, the An-O bonds are the most covalent, and those of the heavier group 4 elements the least. Within the actinide series, Th stands apart from the other three elements considered, being consistently the least covalent, and most like the d transition metals, probably a reflection of the limited 5f contribution to the Th-O interaction. QCT suggests little difference in covalency from Pa-Np, by contrast to the NLMO %M x overlap metric, which indicates a modest periodic increase.

The complex nature of covalency, particularly in the actinides, is good reason to explore metrics which expand our toolkit for quantifying and partitioning covalency from the chemical information within computed molecular electronic structure, and we recommend that the V_{XC} metric be added to this arsenal.

Acknowledgements

We thank the EPSRC for funding (Grant: EP/N022122/1). VB and NK are also grateful to the University of Manchester for computational resources from the Computational Shared Facility and associated support. Data supporting this study are openly available at DOI: 10.17632/hhjb594rhj.1.

References

1 B. Sadhu and M. Dolg, *Inorg. Chem.*, 2019, **58**, 9738–9748.

2 J. Tanti, M. Lincoln and A. Kerridge, *Inorganics*, 2018, **6**, 88.

3 M. J. Tassell and N. Kaltsoyannis, *Dalt. Trans*, 2010, **39**, 6719–6725.

4 I. Kirker and N. Kaltsoyannis, *Dalt. Trans.*, 2011, **40**, 124–131.

5 J. Su, E. R. Batista, K. S. Boland, S. E. Bone, J. A. Bradley, S. K. Cary, D. L. Clark, S. D. Conradson, A. S. Ditter, N. Kaltsoyannis, J. M. Keith, A. Kerridge, S. A. Kozimor, M. W. Löble, R. L. Martin, S. G. Minasian, V. Mocko, H. S. La Pierre, G. T. Seidler, D. K. Shuh, M. P. Wilkerson, L. E. Wolfsberg and P. Yang, *J. Am. Chem. Soc.*, 2018, **140**, 17977–17984.

6 N. Kaltsoyannis, *Inorg. Chem.*, 2013, **52**, 3407–3413.

7 M. P. Kelley, J. Su, M. Urban, M. Luckey, E. R. Batista, P. Yang and J. C. Shafer, *J. Am. Chem. Soc.*, 2017, **139**, 9901–9908.

8 T. Glaser, B. Hedman, K. O. Hodgson and E. I. Solomon, *Acc. Chem. Res.*, 2000, **33**, 859–868.

9 P. L. A. Popelier, in *The Chemical Bond II: 100 Years Old and Getting Stronger*, ed. D. M. P. Mingos, Springer International Publishing, Cham, 2016, pp. 71–117.

10 M. A. Blanco, A. Martín Pendás and E. Francisco, *J. Chem. Theory Comput.*, 2005, **1**, 1096–1109.

11 A. Martin Pendás, E. Francisco and M. A. Blanco, *J. Phys. Chem. A*, 2006, **110**, 12864–12869.

12 A. M. Pendás, M. A. Blanco and E. Francisco, *J. Comput. Chem.*, 2009, **30**, 98–109.

13 A. Martín Pendás, M. A. Blanco and E. Francisco, *J. Chem. Phys.*, 2006, **125**, 184112.

14 S. Grabowsky, A. Genoni and H. B. Bürgi, *Chem. Sci.*, 2017, **8**, 4159–4176.

15 A. M. Pendás, J. L. Casals-Sainz and E. Francisco, *Chem. – A Eur. J.*, 2019, **25**, 309–314.

16 V. E. J. Berryman, Z. J. Whalley, J. J. Shephard, T. Ochiai, A. N. Price, P. L. Arnold, S. Parsons and N. Kaltsoyannis, *Dalt. Trans.*, 2019, **48**, 2939–2947.

17 M. J. Frisch, G. W. Trucks, H. B. Schlegel, G. E. Scuseria, M. A. Robb, J. R. Cheeseman, G. Scalmani, V. Barone, G. A. Petersson, H. Nakatsuji, X. Li, M. Caricato, A. V. Marenich, J. Bloino, B. G. Janesko, R. Gomperts, B. Mennucci, H. P. Hratchian, J. V. Ortiz, A. F. Izmaylov, J. L. Sonnenberg, D. Williams-Young, F. Ding, F. Lipparini, F. Egidi, J. Goings, B. Peng, A. Petrone, T. Henderson, D. Ranasinghe, V. G. Zakrzewski, J. Gao, N. Rega, G. Zheng, W. Liang, M. Hada, M. Ehara, K. Toyota, R. Fukuda, J. Hasegawa, M. Ishida, T. Nakajima, Y. Honda, O. Kitao, H. Nakai, T. Vreven, K. Throssell, J. Montgomery, J. A., J. E. Peralta, F. Ogliaro, M. J. Bearpark, J. J. Heyd, E. N. Brothers, K. N. Kudin, V. N. Staroverov, T. A. Keith, R. Kobayashi, J. Normand, K. Raghavachari, A. P. Rendell, J. C. Burant, S. S. Iyengar, J. Tomasi, M. Cossi, J. M. Millam, M. Klene, C. Adamo, R. Cammi, J. W. Ochterski, R. L. Martin, K. Morokuma, O. Farkas, J. B. Foresman and D. J. Fox, 2016.

18 M. Ernzerhof and G. E. Scuseria, *J. Chem. Phys.*, 1999, **110**, 5029–5036.

19 C. Adamo and V. Barone, *J. Chem. Phys.*, 1999, **110**, 6158–6169.

20 S. Grimme, J. Antony, S. Ehrlich and H. Krieg, *J. Chem. Phys.*, 2010, **132**, 154104.

21 A. D. Becke and E. R. Johnson, *J. Chem. Phys.*, 2005, **123**, 154101.

22 E. R. Johnson and A. D. Becke, *J. Chem. Phys.*, 2005, **123**, 024101.

23 E. R. Johnson and A. D. Becke, *J. Chem. Phys.*, 2006, **124**, 174104.

24 T. H. J. Dunning, *J. Chem. Phys.*, 1989, **90**, 1007–1023.

25 R. A. Kendall, T. H. Dunning and R. J. Harrison, *J. Chem. Phys.*, 1992, **96**, 6796–6806.

26 D. E. Woon and T. H. Dunning, *J. Chem. Phys.*, 1993, **98**, 1358–1371.

27 A. K. Wilson, T. Van Mourik and T. H. Dunning, *J. Mol. Struct. THEOCHEM*, 1996, **388**, 339–349.

28 W. Küchle, M. Dolg, H. Stoll and H. Preuss, *J. Chem. Phys.*, 1994, **100**, 7535–7542.

29 X. Cao and M. Dolg, *J. Mol. Struct. THEOCHEM*, 2004, **673**, 203–209.

30 X. Cao, M. Dolg and H. Stoll, *J. Chem. Phys.*, 2003, **118**, 487–496.

31 J. E. D. Glendening, J. K. Badenhoop, A. E. Reed, J. E. Carpenter, C. R. L. A. Bohmann, C. M. Morales, P. Karafiloglou and F. Weinhold, 2018.

32 T. A. Keith, 2019.

33 P. L. Arnold, A. Prescimone, J. H. Farnaby, S. M. Mansell, S. Parsons and N. Kaltsoyannis, *Angew. Chemie Int. Ed.*, 2015, **54**, 6735–6739.

34 R. E. Wilson, S. De Sio and V. Vallet, *Nat. Commun.*, 2018, **9**, 2–10.

35 J. A. Platts and R. J. Baker, *Dalt. Trans.*, 2020, **49**, 1077–1088.

36 B. D. Cremer and E. Kraka, *Angew. Chem. Int. Ed. Engl*, 1984, **23**, 627–628.

37 C. F. Matta and R. J. Boyd, Eds., *The Quantum Theory of Atoms in Molecules: From Solid State to DNA and Drug Design*, Wiley-VCH, Weinheim, Germany, 2007.

38 M. Ziółkowski, S. J. Grabowski and J. Leszczynski, *J. Phys. Chem. A*, 2006, **110**, 6514–6521.

39 R. Beekmeyer and A. Kerridge, *Inorganics*, 2015, **3**, 482–499.

40 M. Gregson, E. Lu, F. Tuna, E. J. L. McInnes, C. Hennig, A. C. Scheinost, J. McMaster, W. Lewis, A. J. Blake, A. Kerridge and S. T. Liddle, *Chem. Sci.*, 2016, **7**, 3286–3297.

41 A. R. E. Mountain and N. Kaltsoyannis, *Dalt. Trans.*, 2013, **42**, 13477–13486.

42 I. Cukrowski and P. M. Polestshuk, *Phys. Chem. Chem. Phys.*, 2017, **19**, 16375–16386.